NO Rotational Orientation Following 308 nm Photodissociation of NO_2

M. Brouard,* P. O'Keeffe, D. M. Joseph, and D. Minayev

The Physical and Theoretical Chemistry Laboratory, The Department of Chemistry, University of Oxford, South Parks Road, Oxford OX1 3QZ, United Kingdom

(Received 9 November 2000)

The rotational angular momentum orientation and alignment of the NO fragments generated via linearly polarized 308 nm photodissociation of NO_2 has been determined using laser induced fluorescence. By observing the dependence of the photofragment NO Doppler-resolved transition line shapes on experimental geometry, it has proved possible to determine multipole moments of the photofragment angular momentum distribution up to, and including, rank 3. The implications of the results for the mechanism of the dissociation are considered.

DOI: 10.1103/PhysRevLett.86.2249 PACS numbers: 33.80.Gj, 34.50.Gb, 82.50.Hp

The complete description of molecular photodissociation requires knowledge of the correlated distribution between photofragment recoil and angular momentum vectors $\mathbf{v}$ and $\mathbf{j}$ [1–7] (i.e., the recoil angle resolved multipole moments of the density matrix). Interest in measuring angular momentum polarization effects [8–14] has been motivated recently by the fact that photofragment orientation [11,12,14] and alignment [8–10], characterized by multipole moments with odd and even rank k, respectively, are sensitive to quantum mechanical coherence and nonadiabatic effects [4,6,7]. Most studies have probed electronic orbital orientation and alignment in the *atomic* products of diatomic [4,8,11] or triatomic [9,12,14] molecular photodissociation. In the latter case, the atomic products are usually accompanied by *molecular* cofragments, which carry the additional complexity of both rotational and electronic angular momenta. Since the key paper by Dixon [5] on the semiclassical theory of vector correlations in molecular photodissociation, there have been numerous studies of photofragment rotational alignment effects in polyatomic systems [15,16]. However, apart from a few isolated, though notable exceptions [10,13,17], measurement of the angular momentum orientation of molecular photofragments has been largely neglected.

In this Letter we report the rotational orientation and alignment of the NO products generated by *linearly* polarized excimer laser photodissociation of NO_2 at 308 nm. We have determined multipole moments of the NO angular momentum distribution with rank $k \leq 3$ using Doppler-resolved laser induced fluorescence (LIF) [5,18]. The observed photofragment orientation can be rationalized qualitatively in terms of a classical model [13,19], analogous to that used to explain product angular momentum orientation in bimolecular chemical reactions [20], and termed planar or *false chirality* [13,19].

The experimental techniques employed have been described in detail elsewhere [21]. Photodissociation of room temperature samples of NO_2, held at pressures $\leq$50 mTorr, was achieved with pulsed, linearly polarized excimer laser radiation at 308 nm. A portion of the 308 nm beam was employed to pump a frequency doubled dye laser operating around 225 nm, which was used to probe the NO($v = 0, N = 29$) photofragments on the $P_{11}(29)$ transition via the $(0,0)$ band of the $A \leftarrow X$ transition [22]. Spectra of thermalized NO were recorded to verify that the etalon narrowed dye laser radiation was of near-Gaussian line shape, with a full-width-at-half-maximum of 0.08 ± 0.01 cm^{-1}. Unresolved, polarized NO emission was detected via off-diagonal vibronic bands at wavelengths $\gtrsim$230 nm using a combination of photomultiplier and boxcar integrator. The gate delay (with respect to the photolysis pulse) and the gate width of the latter were set at $\sim$20 and $\sim$60 ns, respectively. The optical delay between the pump and probe laser pulses was $\lesssim$20 ns in the interaction region.

The alignment measurements employed linearly polarized pump and probe laser radiation, and the detected emission was viewed through a linear polarizer. Doppler-resolved spectral contours were recorded in eight of the possible twelve pump/probe/detector geometries tabulated by Dixon [5], in which all beam propagation and polarization vectors are fixed at 0° or 90° with respect to the electric vector of the photolysis radiation, ϵ_p (defined as the laboratory Z axis). The direction of ϵ_p was switched through 90° on alternate laser shots using a photoelastic modulator. Odd moments of the angular momentum distribution were determined using the pump-probe geometries illustrated in Fig. 1. Since these measurements rely on detecting elliptically polarized emission, a quarter wave plate was placed in front of the linear polarizer and photomultiplier detector described above [18]. LIF signals sensitive to photofragment orientation were recorded by switching between left and right circular polarizations of the *probe* laser radiation on alternate laser shots.

The Doppler-resolved LIF profile for each geometry $D(\bar{\nu})$ can be represented as a linear combination of *composite Doppler profiles* $D_0^K(k_1, k; \bar{\nu})$ [5,20], each proportional to a single (renormalized) bipolar moment of the correlated angular distribution, $\beta_0^K(k_1, k)$ [5,23]. The weighting coefficients of the linear combination (which are readily evaluated using Ref. [18], together with a generalization of Table I of Dixon [5] to include odd

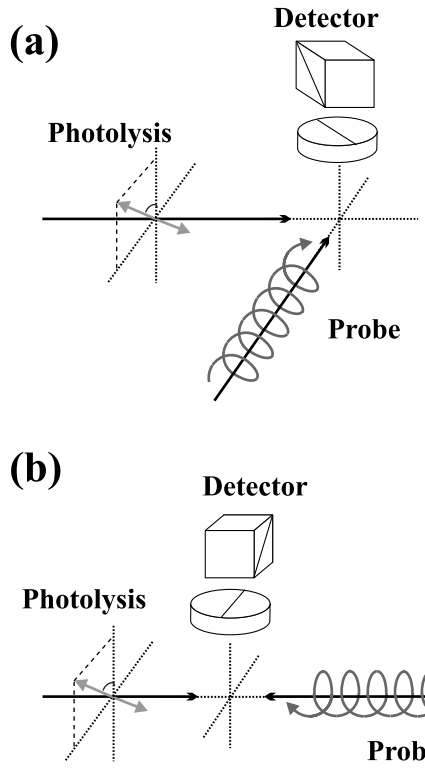

FIG. 1. Experimental geometries used to probe photofragment orientation: (a) the geometry with $\theta_a = \pm 45°$ which is most sensitive to moments of rank $k = 1$, and (b) the geometry with $\theta_a = 90°$ which is sensitive only to $k = 3$ moments. θ_a is the angle between the probe laser propagation direction and the laboratory Z-axis, which lies along $\boldsymbol{\epsilon}_p$.

moments of the angular momentum distribution) vary with rotational transition and experimental geometry [5,18]. The coefficients determine the sensitivity of the experiments to a given bipolar moment [5,10,20].

The sum and difference between NO photofragment Doppler-resolved LIF contours obtained using left and right circularly polarized probe light in the two geometries of Fig. 1 are shown in Figs. 2(a) and 2(b). The summed signals, shown in the left panel of each figure, depend only on the population and alignment of the NO photofragments, while the difference signals, shown on the right, are a direct measure of the angular momentum orientation of the NO photofragments. We have demonstrated that for the geometry shown in Fig. 1(a), the orientation signal disappears, as expected, when $\theta_a = 0°$ or 90°, and changes sign when θ_a is varied from $+45°$ to $-45°$: analogous behavior has been reported by Cline and co-workers using ion imaging techniques [13]. For the particular $P\uparrow$ branch transition in question, the geometry shown in Fig. 1(a) is about $5\times$ more sensitive to moments of order $k = 1$, i.e., to $\beta_0^2(21)$, than to moments with $k = 3$, i.e., to $\beta_0^2(23)$ and $\beta_0^2(43)$. The counterpropagating geometry of Fig. 1(b), on the other hand, is *only* sensitive to moments with $k = 3$ [predominantly $\beta_0^2(23)$], which have weighting coefficients of the same order of magnitude as that for the $k = 1$ moment in geometry of Fig. 1(a). The relative intensities of the difference profiles shown in Figs. 2(a) and 2(b) suggest, therefore, that contributions from the $k = 3$ moments to the photofragment distribution are smaller than that from the $k = 1$ moment.

TABLE I. Values of the bipolar moments for the NO fragments born in $v = 0, N = 29$ generated via the 308 nm photodissociation of NO_2. (N represents the total angular momentum quantum number apart from electron spin.) The numbers in brackets are the Monte Carlo determined errors (2σ) in the last figure given. $\beta_0^2(43)$ was constrained to equal $-\frac{8}{\sqrt{15}}\beta_0^2(23)$ in the fitting procedure. The moments are normalized such that $\beta_0^0(00) = 1$.

$\beta_0^2(20)$	$\beta_0^2(21)$	$\beta_0^2(02)$	$\beta_0^0(22)$	$\beta_0^2(22)$	$\beta_0^2(42)$	$\beta_0^2(23)$
0.61	0.22	−0.23	−0.38	0.27	−0.27	−0.06
(2)	(4)	(2)	(4)	(5)	(8)	(5)

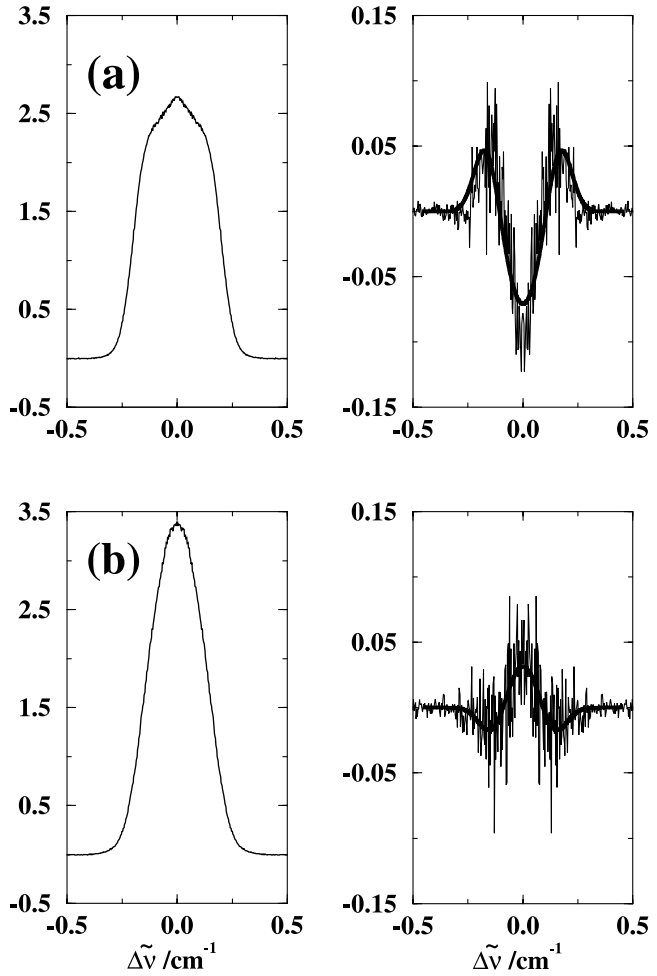

FIG. 2. (a) Sum (left) and difference (right) signals between Doppler-resolved profiles obtained using left and right circular polarized probe laser light in the geometry shown in Fig. 1(a). (b) Analogous sum and difference signals for the geometry shown in Fig. 1(b). The summed signal in each figure depends only on population and alignment, while the difference signal depends only on orientation (see caption to Fig. 1 and text).

The experiments performed with linearly polarized pump, probe, and emitted radiation have allowed the determination of all even moments of the photofragment angular distribution with $k = 0$ and 2, following procedures similar to those described elsewhere [21]. LIF signals were an order of magnitude less sensitive to moments with $k = 4$, and these could not be determined in the present study. Doppler-resolved profiles, including, for example, the summed profiles shown in Fig. 2, were least-squares fit with a set of basis functions which allowed for the thermal motion of the NO_2 parent molecule, and the finite resolution of the probe laser radiation. The only adjustable parameters used in the fitting were the bipolar moments of interest: the returned values are given in Table I, together with their Monte Carlo determined errors. The values reported here for the bipolar moments with even k are consistent with the somewhat more limited set determined previously by Hancock and co-workers [24] for the photolysis of NO_2 at 355 nm: excitation at both 355 and 308 nm are believed to access the $\tilde{A}(^2B_2)$ state [25], which has its transition moment polarized parallel to the terminal oxygen atoms. The greater magnitude of the translational anisotropy, $2\beta_0^2(20)$, obtained in the present thermal measurements, however, suggests a significant reduction in dissociation time at the higher available energy employed here [24].

In the semiclassical limit, when the fragment rotational angular momentum is much greater than that of the parent triatomic molecule, $j \gg J$, the angle between $\mathbf{v}$ and $\mathbf{j}$ must tend to 90° [6]. Under these conditions $\beta_0^0(22) = -\frac{1}{2}$, and $\beta_0^2(42)$ should be constrained to $\frac{7}{12}\beta_0^2(02) - \frac{5}{12}\beta_0^2(22)$ [4,6,10,26,27]. Substituting the values of $\beta_0^2(02)$ and $\beta_0^2(22)$ obtained here (see Table I) into the latter equation yields $\beta_0^2(42) = -0.25$, very close to the value determined by the (unconstrained) fitting procedure. Small deviations of $\beta_0^0(22)$ and $\beta_0^2(42)$ from these limiting values probably reflect the effects of nonzero angular momentum J in the room temperature parent molecule [10]. In the semiclassical limit, the orientation moment $\beta_0^2(43)$ must also be constrained to equal $-\frac{8}{\sqrt{15}}\beta_0^2(23)$ [27]. Least-squares fits to the orientation dependent LIF data shown in Fig. 2, using analogous procedures to those described for the even moments, together with the above constraint on $\beta_0^2(43)$, lead to the values of $\beta_0^2(21)$ and $\beta_0^2(23)$ given in Table I. The best fits to the data are shown as the smooth lines in Fig. 2. Alternative fits, in which we have made the extreme assumption that $\beta_0^2(43) = 0.0$, yield $\beta_0^2(21) = 0.23 \pm 0.05$ and $\beta_0^2(23) = -0.09 \pm 0.05$. The quality of these fits is slightly poorer than those shown in Fig. 2. The fact that the two analyses yield such similar values for the $\beta_0^2(21)$ and $\beta_0^2(23)$ orientation moments is primarily a consequence of the low sensitivity of the present experiments to the effects of $\beta_0^2(43)$.

Semiclassically, each bipolar moment represents the expectation value of the (complex conjugate of the) corresponding bipolar harmonic [5]. Following the renormalization of Dixon [5] and Cline and co-workers [13], the first orientation bipolar moment, $\beta_0^2(21)$, is therefore defined

$$\beta_0^2(21) = -2\langle \sin\theta_t \cos\theta_t \sin\theta_r \sin\phi_r \rangle,$$

with limiting values of ± 1. The angles (θ_i, ϕ_i) are the body fixed frame polar angles of the photofragment translational recoil ($i = t$) and rotational angular momentum ($i = r$) vectors, respectively: the body fixed frame z axis lies along the parent molecule transition moment $\boldsymbol{\mu}$, and the xz plane contains the recoil velocity vector [28]. The positive sign of $\beta_0^2(21)$ observed here implies that fragments recoiling close to the line $x = z$ ($\theta_t \leq 90°$) have angular momenta oriented preferential along the $-y$ direction (i.e., $\phi_r = 3\pi/2$). Conversely, fragments recoiling in the $x = -z$ direction ($\theta_t \geq 90°$) have momenta preferentially oriented along the $+y$ direction. The sign of the orientation moment $\beta_0^2(21)$ is the same as that reported previously in the 355 nm study by Cline and co-workers [13], and in fact its magnitude is also similar to the preliminary value reported in that work [13]. The higher-order odd moment, $\beta_0^2(23)$, has not been determined previously, to our knowledge.

The photofragment angular momentum polarization can be illustrated using the bipolar moments of Table I to evaluate the (semiclassical) angular distribution function $P(\theta_t, \theta_r, \phi_r)$, as shown in Fig. 3. The reconstructed distribution is necessarily truncated, with the moments with $k \geq 4$ that were not determined in the present experiments set equal to zero. The distribution of photofragment angular momentum vectors is shown in the form of a polar plot in the left panels, with the bold arrow representing the direction of recoil, $\mathbf{v}$. The strong rotational alignment along the body fixed y axis, perpendicular to the plane containing $\boldsymbol{\mu}$ and $\mathbf{v}$ (as expected in the semiclassical high j limit discussed above), and the change in orientation of $\mathbf{j}$ with recoil direction, are clearly visible.

The diagrams shown in the panels on the right of Figs. 3 illustrate the types of nuclear motion which might give rise to the polarization behavior described. The orientation signals are consistent with a torque being exerted on the central nitrogen atom during fragmentation. As noted by Cline and co-workers [13], such a torque might be generated simply by the impulsive release of energy along the breaking N-O bond, although it is likely that the mechanism is more complex than this. The $\tilde{A}(^2B_2)$ electronic state to which NO_2 is excited around 300 nm correlates with electronically excited atomic oxygen products (a channel which is closed at the energies supplied to the parent molecule). Dissociation to the products $O(^3P) + NO(^2\Pi)$ is believed to occur via passage through a conical intersection with the ground $\tilde{X}(^2A_1)$ electronic state (see, for example, [25]). The geometry of the excited electronic state [which has a smaller equilibrium bond angle than $NO_2(\tilde{X})$], and the predicted configuration of the conical intersection [25], are

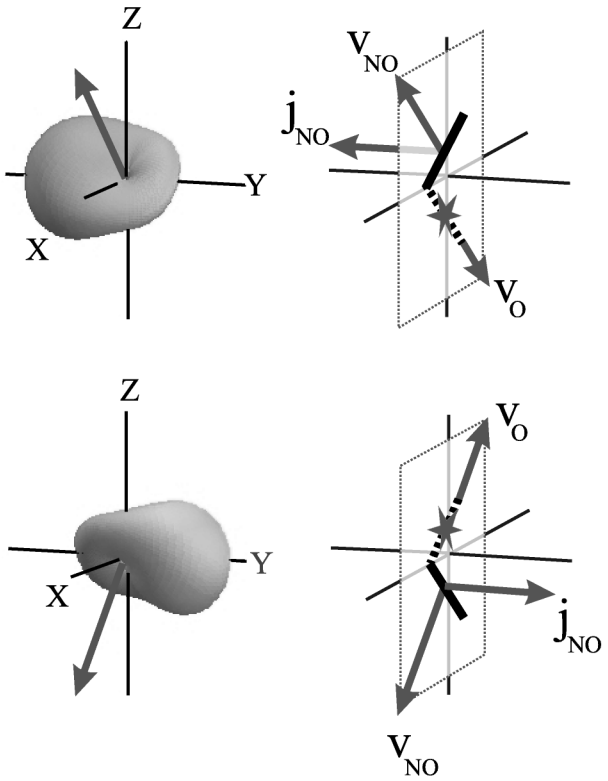

FIG. 3. The distribution $P(\theta_t, \theta_r, \phi_r)$. The polar plots (left panels) show the semiclassical angular distribution of **j** at two recoil angles θ_t (represented by the bold arrow in the left panels) evaluated using the bipolar moments given in Table I. The mutual orientation of the vectors is illustrated schematically in the panels on the right.

both likely to promote NO rotational orientation with the same sense as determined here.

We are very grateful to the EPSRC for a research grant which funded D. M. J. and P. O'K. Support from the Royal Society is also acknowledged. We are grateful to Professor F. Javier Aoiz and Professor Oleg S. Vasyutinskii for valuable discussions.

*Email address: mark.brouard@chemistry.ox.ac.uk

[1] U. Fano and J. H. Macek, Rev. Mod. Phys. **45**, 553 (1973).
[2] D. A. Case, G. M. McClelland, and D. R. Herschbach, Mol. Phys. **35**, 541 (1978).
[3] C. H. Greene and R. N. Zare, Annu. Rev. Phys. Chem. **33**, 119 (1982).
[4] O. S. Vasyutinskii, Opt. Spektrosk. **54**, 524 (1983); B. V. Picheyev, A. G. Smolin, and O. S. Vasyukinskii, J. Phys. Chem. **101**, 7614 (1997).
[5] R. N. Dixon, J. Chem. Phys. **85**, 1866 (1986).
[6] L. D. A. Siebbeles, M. Glass-Maujean, O. S. Vasyutinskii, J. A. Beswick, and O. Roncero, J. Chem. Phys. **100**, 3610 (1994).
[7] A. Pe'er, M. Shapiro, and G. G. Balint-Kurti, J. Chem. Phys. **110**, 11 928 (1999).
[8] A. S. Bracker, E. R. Wouters, A. G. Suits, Y. T. Lee, and O. S. Vasyutinskii, Phys. Rev. Lett. **80**, 1626 (1998).
[9] M. Ahmed, D. S. Peterka, A. S. Bracker, O. S. Vasyutinskii, and A. G. Suits, J. Chem. Phys. **110**, 4115 (1999); M. Ahmed, E. R. Wouters, D. S. Peterka, O. S. Vasyutinskii, and A. G. Suits, Faraday Discuss. Chem. Soc. **113**, 425 (1999).
[10] M. L. Costen, S. W. North, and G. E. Hall, J. Chem. Phys. **111**, 6735 (1999); M. L. Costen, Faraday Discuss. Chem. Soc. **113**, 481 (1999).
[11] T. P. Rakitzis, S. A. Kandel, A. J. Alexander, Z. H. Kim, and R. N. Zare, Science **281**, 1346 (1998); J. Chem. Phys. **110**, 3351 (1999); Z. H. Kim, A. J. Alexander, S. A. Kandel, T. P. Rakitzis, and R. N. Zare, Faraday Discuss. Chem. Soc. **113**, 27 (1999).
[12] Z. H. Kim, A. J. Alexander, and R. N. Zare, J. Phys. Chem. **103**, 10 144 (1999).
[13] V. K. Nestorov and J. I. Cline, J. Chem. Phys. **111**, 5287 (1999).
[14] T. P. Rakitzis, P. C. Samartzis, and T. N. Kitsopoulos, J. Chem. Phys. **111**, 10 415 (1999).
[15] J. P. Simons, J. Phys. Chem. **91**, 5378 (1987).
[16] P. L. Houston, J. Phys. Chem. **91**, 5388 (1997).
[17] E. Hasselbrink, J. R. Waldeck, and R. N. Zare, Chem. Phys. **126**, 191 (1988); J. F. Black, E. Hasselbrink, J. R. Waldeck, and R. N. Zare, Mol. Phys. **71**, 1143 (1990).
[18] A. C. Kummel, G. O. Sitz, and R. N. Zare, J. Chem. Phys. **88**, 7357 (1988).
[19] R. Uberna, R. D. Hinchliffe, and J. I. Cline, J. Chem. Phys. **103**, 1934 (1995).
[20] F. J. Aoiz, M. Brouard, and P. A. Enriquez, J. Chem. Phys. **105**, 4964 (1996); F. J. Aoiz, M. Brouard, V. J. Herrero, V. Sáez Rábanos, and K. Stark, Chem. Phys. Lett. **264**, 487 (1997).
[21] M. Brouard, S. Gatenby, D. M. Joseph, and C. Vallance, J. Chem. Phys. **113**, 3162 (2000).
[22] J. Luque and D. R. Crosley, SRI International Report No. MP 99-009, 1999.
[23] The composite Doppler profiles $D_0^K(k_1, k; \bar{\nu})$ have a $P_{k_1}(\chi_D)$ dependence on the relative Doppler shift from the line center, χ_D, and hence on probe laser frequency $\bar{\nu}$ [5,20]. $P_{k_1}(\cdots)$ are the Legendre polynomials.
[24] R. P. Baker, M. L. Costen, G. Hancock, and G. A. D. Ritchie, Phys. Chem. Chem. Phys. **2**, 661 (2000).
[25] H. Katagiri and S. Kato, J. Chem. Phys. **99**, 8805 (1993).
[26] T. P. Rakitzis, G. E. Hall, M. L. Costen, and R. N. Zare, J. Chem. Phys. **111**, 8751 (1999).
[27] The constraints on $\beta_0^2(42)$ and $\beta_0^2(43)$ may be obtained by setting the coherent term $f_2(1, 0)$ and $f_3(1, -1)$ in Eqs. B6 and B7 of Siebbeles *et al.* to zero [6,10].
[28] With this definition of body fixed frame, $\phi_t = 0$.